

GaussianFormer-2: Probabilistic Gaussian Superposition for Efficient 3D Occupancy Prediction

Yuanhui Huang¹ Amonnut Thammatadatrakoon¹ Wenzhao Zheng^{1,*}

Yunpeng Zhang² Dalong Du^{1,2} Jiwen Lu¹

¹Tsinghua University, China ²PhiGent Robotics

{huangyh22, yam23}@mails.tsinghua.edu.cn; wenzhao.zheng@outlook.com

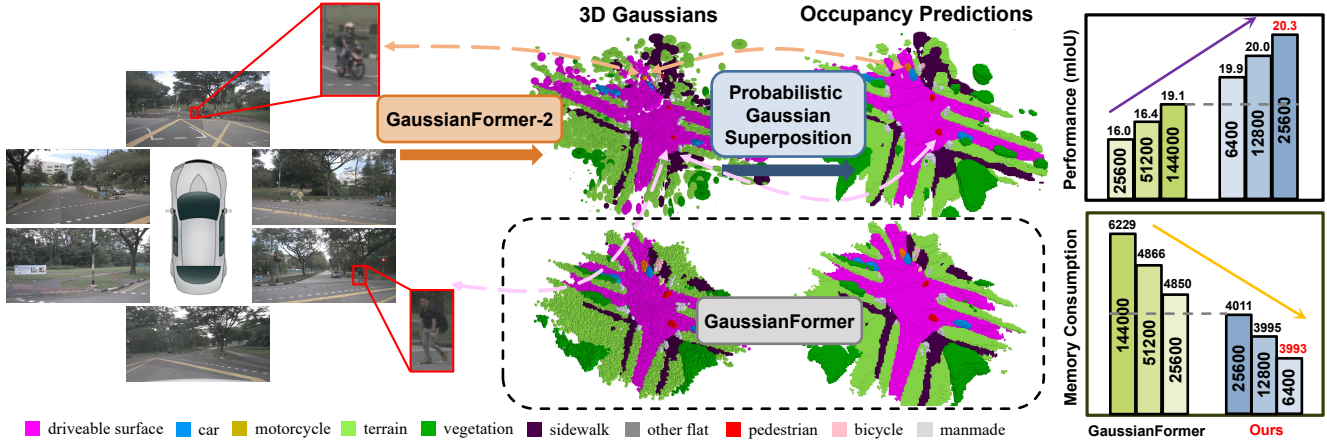


Figure 1. We approach efficient object-centric scene representation from a probabilistic perspective and propose the probabilistic Gaussian superposition model, which achieves SOTA performance with as few as 8.9% of Gaussians in GaussianFormer [15].

Abstract

3D semantic occupancy prediction is an important task for robust vision-centric autonomous driving, which predicts fine-grained geometry and semantics of the surrounding scene. Most existing methods leverage dense grid-based scene representations, overlooking the spatial sparsity of the driving scenes. Although 3D semantic Gaussian serves as an object-centric sparse alternative, most of the Gaussians still describe the empty region with low efficiency. To address this, we propose a probabilistic Gaussian superposition model which interprets each Gaussian as a probability distribution of its neighborhood being occupied and conforms to probabilistic multiplication to derive the overall geometry. Furthermore, we adopt the exact Gaussian mixture model for semantics calculation to avoid unnecessary overlapping of Gaussians. To effectively initialize Gaussians in non-empty region, we design a distribution-based initialization module which learns the pixel-aligned occupancy distribution instead of the depth of surfaces. We conduct extensive experiments on nuScenes and KITTI-360 datasets and our GaussianFormer-2 achieves state-of-the-art performance with high efficiency. Code: <https://github.com/huang-yh/GaussianFormer>.

1. Introduction

In autonomous driving, vision-centric systems have been more cost-effective compared with the LiDAR-based coun-

terparts. However, their inability to capture obstacles with arbitrary shapes poses challenges for driving safety and reliability [11, 16, 20, 23]. The advent of 3D semantic occupancy prediction methods [3, 13, 17, 22, 24, 31, 44, 51] alleviates this limitation by predicting the fine-grained geometry and semantics of the surrounding 3D environment. This advancement supports a range of emerging applications, including end-to-end autonomous driving [11, 40], 4D occupancy forecasting [42, 47, 52], and self-supervised 3D scene understanding [4, 14, 45].

Despite the promising applications, 3D semantic occupancy prediction is essentially a dense three-dimensional segmentation task [3, 39], which necessitates a both efficient and effective representation of the 3D scene. Voxel-based methods [22, 44] use dense 3D voxels as representation to describe the scene with the finest detail. However, they neglect the spatial redundancy of the 3D occupancy and suffer from high computational complexity. As a workaround, planer representations, such as BEV [23, 50] and TPV [13], compress the 3D grid along one of the axes to derive 2D feature maps for reduction of the token number. Nonetheless, they still take into account the empty region when modeling the environment, which compromises their model capacity and efficiency. As a pioneer in object-centric sparse scene representations, 3D semantic Gaussians [15] describe the 3D space in a sparse way with learnable mean, covariance, opacity and semantics for each Gaussian. However, several limitations persist in the current 3D semantic Gaussian representation: 1) Each Gaussian can still describe the empty region, which renders most of the

*Project leader.

Gaussians useless in an object-centric formulation given the spacial sparsity of 3D occupancy. 2) The aggregation process ignores the overlapping issue and directly sums up the contribution of each Gaussian to produce occupancy prediction, which results in unbounded semantic logits and further increases the overlapping among Gaussians. Thus, the proportion of effective Gaussians describing occupied regions independently could be extremely low, which undermines the efficiency of the 3D semantic Gaussian representation.

In this paper, we introduce a probabilistic Gaussian superposition model to resolve the above limitations of 3D semantic Gaussians and improve utilization and efficiency. To elaborate, we propose the probabilistic Gaussian representation, which assigns 3D Gaussians to exclusively model the non-empty area by interpreting each Gaussian as a probability distribution of its neighborhood being occupied. We employ the multiplication theorem of probability to aggregate the independent probability distributions and derive the geometry predictions. Furthermore, we integrate the Gaussian mixture model into our probabilistic Gaussian representation to generate normalized semantic predictions, which avoid unbounded logits and prevents Gaussians from unnecessary overlapping. Since our representation only models the occupied region, we also design a distribution-based initialization module to effectively initialize Gaussians around the non-empty area, which learns the pixel-aligned occupancy distribution instead of depth values of surfaces [12, 20, 22]. We conduct extensive experiments on the nuScenes [2] and KITTI-360 [26] datasets for surround-view and monocular 3D semantic occupancy prediction, respectively. Our GaussianFormer-2 outperforms state-of-the-art methods with high efficiency. In addition, qualitative visualizations show that GaussianFormer-2 is able to generate a both holistic and realistic perception of the scene.

2. Related Work

3D Semantic Occupancy Prediction. 3D semantic occupancy prediction [3, 13, 39] has emerged as a promising environment modeling in autonomous driving as it describes driving scenes in a comprehensive manner. This task aims to label each voxel in the scene by taking one or more types of sensors as input. Two most used sensors are LiDAR and the camera. Although LiDAR-based methods perform remarkably well in 3D perception tasks [3, 5, 6, 8, 18, 19, 27, 34, 37, 46, 48, 49, 53], they possess limitations under bad weather conditions and in detecting distant objects; Thus, camera-based approaches have garnered increasing attention [24, 44, 50]. Pioneer works in 3D semantic occupancy prediction task adopt dense grid-based representation as a straightforward mean to derive occupancy [7, 22, 44], then subsequent works turn to sparse object-centric representation [15, 30, 38] as a solution to the innate problem of redundancy for dense representations.

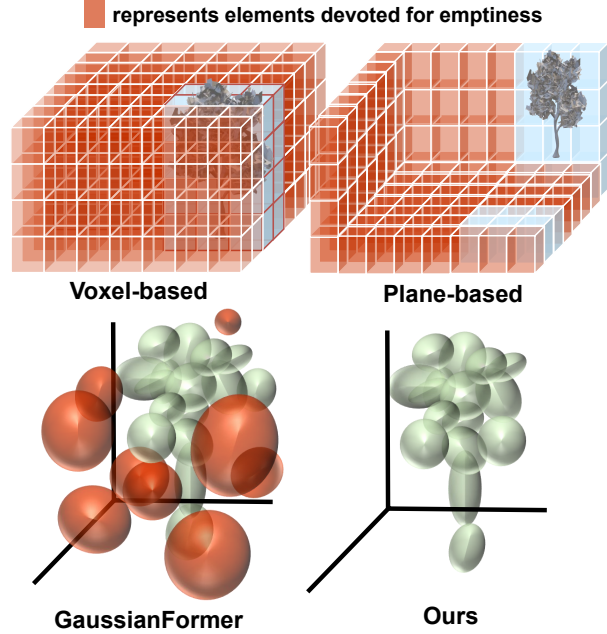


Figure 2. **Representation comparisons.** Voxel and plane based representations inevitably incorporate emptiness when modeling the 3D scene. While GaussianFormer [15] proposes 3D semantic Gaussian as a sparse representation, it still suffer from spatial redundancy. Our method achieves true object-centricity through probabilistic modeling.

Grid-based scene representations. Plane representations have emerged as competitive representations in scene perception tasks for autonomous driving. BEVFormer [23] is the initiative work of the kind [12, 20, 25, 28, 33] that utilizes only camera input and performs comparably well with LiDAR-based methods in detection and segmentation tasks. It converts the image feature to the bird’s-eye-view (BEV) feature as a unified scene representation, since the information is most diverse at this point of view. The BEV feature is then used for downstream tasks. However, the BEV feature is not suitable for 3D occupancy construction as it causes height information to be lost [44]. As a generalization of BEV space, TPVFormer [13] proposes tri-perspective view representation to include also the height information, thus making it more suitable for 3D scenes. Another research direction [22, 44] adopts voxel-based representation as a more 3D-specific and fine-grained approach, making it favorable for 3D volumetric semantic prediction. Nevertheless, these methods utilize dense grid-based representation, which describes each voxel equally regardless of the spatial sparsity of the environment, thus resulting in intrinsic redundancy.

Object-centric scene representations. To eliminate spatial redundancy inherent in dense representations, many recent works adopt sparse representation [15, 30, 38]. One line of work divides dense grids into partitions where objects present and omits the regions foreseen as empty [30, 38]. However, non-empty regions might be mistakenly clas-

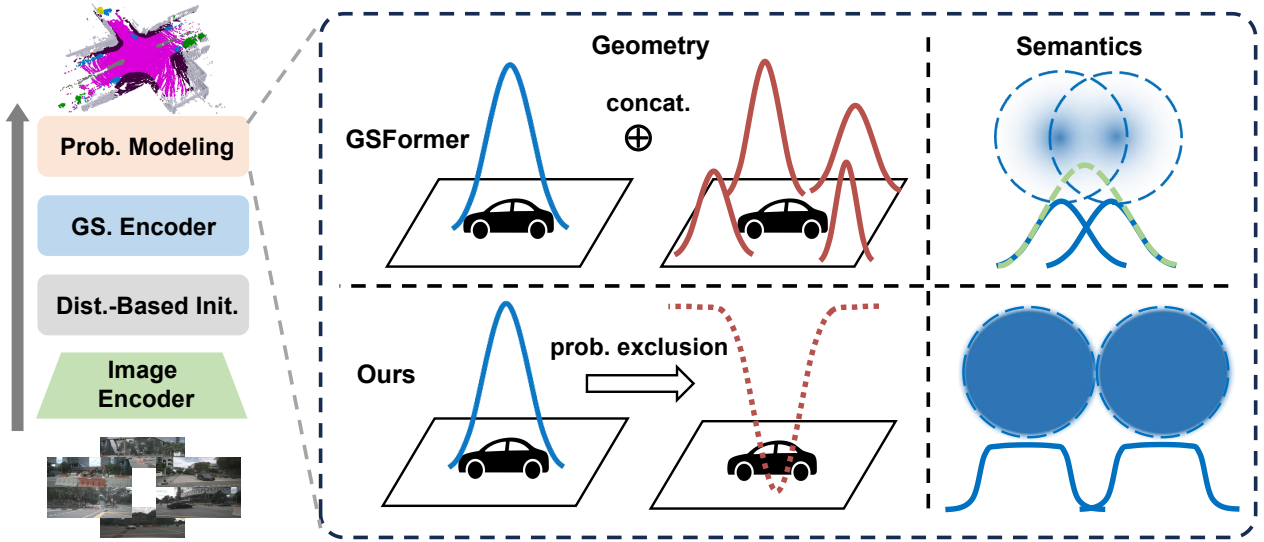


Figure 3. **Overall pipeline of our method.** To achieve probabilistic modeling, we decompose occupancy prediction into geometry and semantics prediction, and approach them separately using probabilistic multiplication and Gaussian mixture model to improve efficiency.

sified as unoccupied and eliminated completely from the whole subsequent process. Another line of work leverages point representation [35, 41] by sampling points within the scene range as queries in the succeeding refinement process; Nevertheless, a point has a limited range of depiction as it has no spatial extent. An alternative approach, GaussianFormer [15], adopts 3D semantic Gaussian representation, where probability spreads around a mean, allowing more utilization. However, spatial redundancy persists due to no regulation for the Gaussians to not represent emptiness.

3. Proposed Approach

In this section, we present our method of probabilistic Gaussian superposition for efficient 3D semantic occupancy prediction. We first review the original 3D semantic Gaussian representation [15] and its limitations (Sec. 3.1). We then introduce our probabilistic Gaussian modeling and how we derive geometry and semantics predictions based on the multiplication theorem of probability and Gaussian mixture model (Sec. 3.2). Finally, we detail the distribution-based initialization module to effectively initialize probabilistic Gaussians around the occupied area (Sec. 3.3).

3.1. 3D Semantic Gaussian Representation

Vision-centric 3D semantic occupancy prediction [3, 13] aims to obtain the fine-grained geometry and semantics of the 3D scene. To formulate, the target is to predict voxel-level semantic segmentation result $\mathbf{O} \in \mathcal{C}^{X \times Y \times Z}$ given input images $\mathcal{I} = \{\mathbf{I}_i\}_{i=1}^N$, where $\mathcal{C}, \{X, Y, Z\}, N$ represent the set of predefined classes, the spatial resolution of occupancy and the number of input views, respectively.

To achieve this, 3D semantic Gaussian representation employs a set of P Gaussian primitives $\mathcal{G} = \{\mathbf{G}_i\}_{i=1}^P$,

with each \mathbf{G}_i describing a local region with its mean \mathbf{m}_i , scale \mathbf{s}_i , rotation \mathbf{r}_i , opacity a_i and semantics \mathbf{c}_i . GaussianFormer interprets these primitives as local semantic Gaussian distributions which contribute to the overall occupancy prediction through additive aggregation:

$$\hat{\mathbf{o}}(\mathbf{x}; \mathcal{G}) = \sum_{i=1}^P \mathbf{g}_i(\mathbf{x}; \mathbf{m}_i, \mathbf{s}_i, \mathbf{r}_i, a_i, \mathbf{c}_i), \quad (1)$$

where $\mathbf{g}_i(\mathbf{x}; \cdot)$ denotes the contribution of the i th semantic Gaussian to $\hat{\mathbf{o}}(\mathbf{x}; \mathcal{G})$ which is the overall occupancy prediction at location \mathbf{x} . The contribution \mathbf{g} is further calculated as the corresponding semantic Gaussian distribution evaluated at location \mathbf{x} :

$$\mathbf{g}(\mathbf{x}; \mathbf{G}) = a \cdot \exp\left(-\frac{1}{2}(\mathbf{x} - \mathbf{m})^T \Sigma^{-1} (\mathbf{x} - \mathbf{m})\right) \mathbf{c}, \quad (2)$$

$$\Sigma = \mathbf{R} \mathbf{S}^T \mathbf{R}^T, \quad \mathbf{S} = \text{diag}(\mathbf{s}), \quad \mathbf{R} = q2r(\mathbf{r}), \quad (3)$$

where Σ , \mathbf{R} , \mathbf{S} represent the covariance matrix, the rotation matrix constructed from the quaternion \mathbf{r} with function $q2r(\cdot)$, and the diagonal scale matrix from function $\text{diag}(\cdot)$.

Although the number of Gaussians is reduced compared with the number of dense voxels thanks to the deformable nature of Gaussian distributions as in Eq. (2), several limitations still persist in the 3D semantic Gaussian representation. First of all, it models both the occupied and unoccupied regions in the same way using the semantic property \mathbf{c} , resulting in most Gaussians being classified as empty given the huge proportion of empty space in outdoor scenarios. Secondly, the semantic Gaussian representation encourages Gaussians to overlap, because the aggregation process in Eq. (1) independently sums up the contribution of each Gaussian, resulting in unbounded occupancy prediction $\hat{\mathbf{o}}$. For optimization, the model would learn to allocate more

Gaussians to describe the same region due to the unbounded nature of $\hat{\mathbf{o}}$, aggravating the overlap between Gaussians. These limitations stem from the current interpretation of Gaussians and obstruct the efficiency and effectiveness of the 3D semantic Gaussian representation. Our method approaches Gaussian-based object-centric representation from a probabilistic perspective, serving as a fundamental solution to these issues, as shown by Figure 2.

3.2. Probabilistic Gaussian Superposition

We propose the probabilistic Gaussian superposition as an efficient and effective 3D scene representation. As shown in Figure 3, we decompose the 3D modeling target into geometry and semantics predictions, and adopt the multiplication theorem of probability and the Gaussian mixture model to address them from a probabilistic perspective, respectively.

Geometry prediction. To restrict Gaussians to represent only occupied regions for geometry prediction, we interpret the Gaussian primitives $\mathcal{G} = \{\mathbf{G}_i\}_{i=1}^P$ as the probability of their surrounding space being occupied. To elaborate, we assign a probability value of 100% at the centers of Gaussians, which decays exponentially with respect to the distance from the centers \mathbf{m} :

$$\alpha(\mathbf{x}; \mathbf{G}) = \exp\left(-\frac{1}{2}(\mathbf{x} - \mathbf{m})^T \Sigma^{-1} (\mathbf{x} - \mathbf{m})\right), \quad (4)$$

where $\alpha(\mathbf{x}; \mathbf{G})$ denotes the probability of the point \mathbf{x} being occupied induced by Gaussian \mathbf{G} . Eq. (4) assigns a high probability of occupancy when the point \mathbf{x} is close to the center of Gaussian \mathbf{G} , which prevents any Gaussian from describing empty area. To further derive the overall probability of occupancy, we assume that the probabilities of a point being occupied by different Gaussians are mutually independent, and thus we can aggregate them according to the multiplication theorem of probability:

$$\alpha(\mathbf{x}) = 1 - \prod_{i=1}^P (1 - \alpha(\mathbf{x}; \mathbf{G}_i)), \quad (5)$$

where $\alpha(\mathbf{x})$ represents the overall probability of occupancy at point \mathbf{x} . In addition to achieving object-centric properties, Eq. (5) also avoids unnecessary overlapping between Gaussians because $\alpha(\mathbf{x}) \geq \alpha(\mathbf{x}; \mathbf{G}_i)$ holds for any Gaussian \mathbf{G}_i . This implies that point \mathbf{x} would be predicted occupied if it is close enough to any single Gaussian.

Semantics prediction. In addition to object-centric anti-overlapping geometry modeling, we still need to achieve the same goals for semantics prediction. We first remove the channel that represents the empty class from the semantic properties \mathbf{c} of Gaussians since it has been accounted for in geometry prediction. Then we interpret the set of Gaussians \mathcal{G} as a Gaussian mixture model, where semantics prediction could be formulated as calculating the expectation of semantics given the probabilistic Gaussian mixture model.

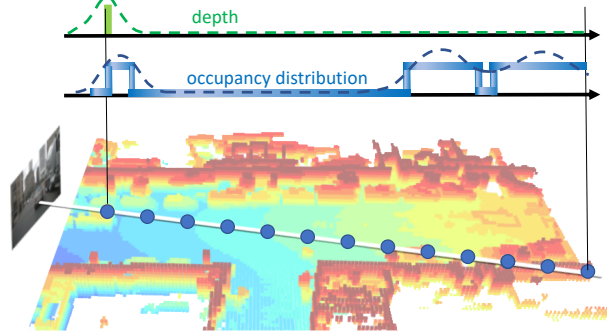


Figure 4. **Distribution-based initialization.** Our initialization scheme learns pixel-aligned occupancy distributions from occupancy annotation, while the depth-based counterpart only captures the surfaces of objects and relies on LiDAR supervision.

Specifically, we take the original opacity properties a as the prior distribution of Gaussians, which is l^1 -normalized. Furthermore, we adopt the Gaussian probabilistic distribution parameterized by mean \mathbf{m} , scale Σ and rotation \mathbf{r} as the conditional probability. Then we normalize the original semantics properties \mathbf{c} with softmax to ensure the boundedness of predicted semantics. Finally, we calculate the expectation $\mathbf{e}(\mathbf{x}; \mathcal{G})$ as:

$$\mathbf{e}(\mathbf{x}; \mathcal{G}) = \sum_{i=1}^P p(\mathbf{G}_i | \mathbf{x}) \tilde{\mathbf{c}}_i = \frac{\sum_{i=1}^P p(\mathbf{x} | \mathbf{G}_i) a_i \tilde{\mathbf{c}}_i}{\sum_{j=1}^P p(\mathbf{x} | \mathbf{G}_j) a_j}, \quad (6)$$

$$p(\mathbf{x} | \mathbf{G}_i) = \frac{1}{(2\pi)^{\frac{3}{2}} |\Sigma|^{\frac{1}{2}}} \exp\left(-\frac{1}{2}(\mathbf{x} - \mathbf{m})^T \Sigma^{-1} (\mathbf{x} - \mathbf{m})\right), \quad (7)$$

where $p(\mathbf{G}_i | \mathbf{x})$, $p(\mathbf{x} | \mathbf{G}_i)$ and $\tilde{\mathbf{c}}_i$ denote the posterior probability of point \mathbf{x} belonging to the i th Gaussian distribution, the conditional probability of point \mathbf{x} given the i th Gaussian distribution, and the softmax-normalized semantic properties, respectively. Compared with Eq. (1)(2), the gaussian mixture model in Eq. (6) normalizes the semantic properties and the contributions from different Gaussians, thus preventing unnecessary overlapping between Gaussians and producing normalized class probabilities directly.

Given the geometry and semantics predictions, we take a simple step forward to combine them to generate the final semantic occupancy prediction:

$$\hat{\mathbf{o}}(\mathbf{x}; \mathcal{G}) = [1 - \alpha(\mathbf{x}); \alpha(\mathbf{x}) \cdot \mathbf{e}(\mathbf{x}; \mathcal{G})], \quad (8)$$

where we use the geometry probability $\alpha(\mathbf{x})$ to weight the semantic predictions, and directly take $1 - \alpha(\mathbf{x})$ as the probability of the empty class.

3.3. Distribution-Based Initialization

Previous 3D semantic Gaussian representation adopts a learnable initialization strategy, which randomly initializes the properties of Gaussians at the beginning of training, and optimizes this initialization in a data-driven way. This strategy enables the model to learn a prior distribution of occupancy of the whole dataset, which relies on the subsequent

Table 1. **Surround view 3D semantic occupancy prediction results on nuScenes.** * means supervised by dense occupancy annotations as opposed to original LiDAR segmentation labels. Ch. denotes the channel dimension of our model. Our method achieves state-of-the-art performance compared with other methods.

Method	IoU	mIoU																		
			barrier	bicycle	bus	car	const. veh.	motorcycle	pedestrian	traffic cone	trailer	truck	drive. suf.	other flat	sidewalk	terrain	manmade	vegetation		
MonoScene [3]	23.96	7.31	4.03	0.35	8.00	8.04	2.90	0.28	1.16	0.67	4.01	4.35	27.72	5.20	15.13	11.29	9.03	14.86		
Atlas [32]	28.66	15.00	10.64	5.68	19.66	24.94	8.90	8.84	6.47	3.28	10.42	16.21	34.86	15.46	21.89	20.95	11.21	20.54		
BEVFormer [23]	30.50	16.75	14.22	6.58	23.46	28.28	8.66	10.77	6.64	4.05	11.20	17.78	37.28	18.00	22.88	22.17	13.80	22.21		
TPVFormer [13]	11.51	11.66	16.14	7.17	22.63	17.13	8.83	11.39	10.46	8.23	9.43	17.02	8.07	13.64	13.85	10.34	4.90	7.37		
TPVFormer* [13]	30.86	17.10	15.96	5.31	23.86	27.32	9.79	8.74	7.09	5.20	10.97	19.22	38.87	21.25	24.26	23.15	11.73	20.81		
OccFormer [51]	31.39	19.03	18.65	10.41	23.92	30.29	10.31	14.19	13.59	10.13	12.49	20.77	38.78	19.79	24.19	22.21	13.48	21.35		
SurroundOcc [44]	31.49	20.30	20.59	11.68	28.06	30.86	10.70	15.14	14.09	12.06	14.38	22.26	37.29	23.70	24.49	22.77	14.89	21.86		
GaussianFormer [15]	29.83	19.10	19.52	11.26	26.11	29.78	10.47	13.83	12.58	8.67	12.74	21.57	39.63	23.28	24.46	22.99	9.59	19.12		
Ours (Ch. = 128)	30.56	20.02	20.15	12.99	27.61	30.23	11.19	15.31	12.64	9.63	13.31	22.26	39.68	23.47	25.62	23.20	12.25	20.73		
Ours (Ch. = 192)	31.74	20.82	21.39	13.44	28.49	30.82	10.92	15.84	13.55	10.53	14.04	22.92	40.61	24.36	26.08	24.27	13.83	21.98		

refinement of the network to adapt to the distribution of each individual sample. However, the local receptive field of Gaussians limits their mobility, which hinders each Gaussian from learning the path to the correct position in subsequent refinement. And this issue is even more severe for our probabilistic Gaussian superposition where Gaussians are supposed to model only occupied regions.

To remedy this issue, we propose a distribution-based initialization module which provides both more accurate and holistic sample-specific initialization for Gaussians, as shown by Figure 4. We supervise the image features from a 2D backbone with the pixel-aligned occupancy distribution derived from the occupancy annotations. To elaborate, we first determine the origin \mathbf{b} and direction \mathbf{d} of the ray corresponding to each image feature with the camera calibration data. We then sample R reference points at equal intervals in a fixed depth range along this ray. For each of these reference points, we query the ground truth occupancy \mathbf{O} at the corresponding location to obtain the binary labels $\mathbf{l} = \{\mathbf{l}_i\}_{i=1}^R$ indicating whether a reference point is occupied or not. Then we use $\mathbf{l} = \{\mathbf{l}_i\}_{i=1}^R$ as supervision to optimize our initialization module, which consists of an image backbone B and a distribution predictor M . The distribution predictor M directly decodes image features into occupancy distributions $\hat{\mathbf{l}}$ along corresponding rays, which are matched against \mathbf{l} using binary cross entropy loss:

$$\text{loss}_{\text{init}} = \text{BCE}(\hat{\mathbf{l}}, \mathbf{l}) = \text{BCE}(M(B(\mathcal{I})), \mathbf{l}). \quad (9)$$

Different from previous initialization schemes [12, 20, 22] that predict the depth values with LiDAR supervision, our method learns the holistic occupancy distribution rather than only visible surfaces of the scene, and does not require any additional modality as supervision.

Overall, our distribution-based initialization module initializes the Gaussians, which are subsequently sent into

B blocks of attention-based architecture as in GaussianFormer [15]. Each block consists of self-encoding, image cross-attention, and refinement module, where probabilistic Gaussian properties steadily improve, then the resulting Gaussians are aggregated by our new method that encourages higher utilization of Gaussians.

4. Experiments

4.1. Datasets and Metrics

The **nuScenes dataset** [2] provides 1000 scenes of surround view driving scenes in Boston and Singapore. The official division is 700/150/150 scenes for training, validation, and testing, respectively. Each scene is 20 seconds long and fully annotated at 2Hz with ground truth from 5 radars, 6 cameras, one LiDAR, and one IMU. We employ 3D semantic occupancy annotations from SurroundOcc [44] for supervision and evaluation. The ranges of the occupancy annotations in the x, y, and z axes in meters are [-50, 50], [-50, 50], and [-5, 3], respectively, where each voxel has a side length of 0.5 meters and is labeled as one of the 18 possible classes (16 semantics, 1 empty, and 1 noise class).

The **KITTI-360 dataset** [26] consists of over 320k images in suburban area with rich 360 degree sensory ground truth, consisting of 2 perspective cameras, 2 fisheye cameras, a Velodyne LiDAR, and a laser scanner, where we use the images from the left camera of the ego car as input to our model. For 3D semantic occupancy prediction, we adopt the annotations from SSCBench-KITTI-360 [21]. The official split is 7/1/1 sequences with 8487/1812/2566 key frames for training, validation, and testing, respectively. The voxel grid area covers $51.2 \times 51.2 \times 6.4 \text{ m}^3$ in front of the ego car with resolution of $256 \times 256 \times 32$. Each voxel is classified as one of the 19 classes (18 semantics and 1 empty).

The **evaluation metrics** are in accordance with common practice [3], namely mean Intersection-over-Union (mIoU)

Table 2. **Monocular 3D semantic occupancy prediction results on SSCBench-KITTI-360.** Our method achieves state-of-the-art performance compared with other methods, surpassing GaussianFormer [15] by a clear margin.

Method	Input	IoU	mIoU	Category IoU																	
				car	bicycle	motorcycle	truck	other-veh.	person	road	parking	sidewalk	other-grnd	building	fence	vegetation	terrain	pole	traf-sign	other-struct.	other-object
LMSCNet [34]	L	47.53	13.65	20.91	0	0	0.26	0	0	62.95	13.51	33.51	0.2	43.67	0.33	40.01	26.80	0	0	3.63	0
SSCNet [36]	L	53.58	16.95	31.95	0	0.17	10.29	0.58	0.07	65.7	17.33	41.24	3.22	44.41	6.77	43.72	28.87	0.78	0.75	8.60	0.67
MonoScene [3]	C	37.87	12.31	19.34	0.43	0.58	8.02	2.03	0.86	48.35	11.38	28.13	3.22	32.89	3.53	26.15	16.75	6.92	5.67	4.20	3.09
Voxformer [22]	C	38.76	11.91	17.84	1.16	0.89	4.56	2.06	1.63	47.01	9.67	27.21	2.89	31.18	4.97	28.99	14.69	6.51	6.92	3.79	2.43
TPVFormer [13]	C	40.22	13.64	21.56	1.09	1.37	8.06	2.57	2.38	52.99	11.99	31.07	3.78	34.83	4.80	30.08	17.51	7.46	5.86	5.48	2.70
OccFormer [51]	C	40.27	13.81	22.58	0.66	0.26	9.89	3.82	2.77	54.30	13.44	31.53	3.55	36.42	4.80	31.00	19.51	7.77	8.51	6.95	4.60
GaussianFormer [15]	C	35.38	12.92	18.93	1.02	4.62	18.07	7.59	3.35	45.47	10.89	25.03	5.32	28.44	5.68	29.54	8.62	2.99	2.32	9.51	5.14
Ours	C	38.37	13.90	21.08	2.55	4.21	12.41	5.73	1.59	54.12	11.04	32.31	3.34	32.01	4.98	28.94	17.33	3.57	5.48	5.88	3.54

and Intersection-over-Union (IoU):

$$\text{mIoU} = \frac{1}{|\mathcal{C}'|} \sum_{i \in \mathcal{C}'} \frac{TP_i}{TP_i + FP_i + FN_i}, \quad (10)$$

$$\text{IoU} = \frac{TP_{\neq c_0}}{TP_{\neq c_0} + FP_{\neq c_0} + FN_{\neq c_0}}, \quad (11)$$

Where \mathcal{C}' , c_0 , TP, FP, and FN represent the non-empty classes, the empty class, and the number of true positive, false positive, and false negative predictions, respectively.

4.2. Implementation Details

The input images are at resolutions of 900×1600 for nuScenes [2] and 376×1408 for KITTI-360 [26] with random flipping and photometric distortion augmentations. We use the same checkpoints for our image backbone as used in GaussianFormer [15], i.e. ResNet101-DCN [10] with FCOS3D checkpoint [43] for nuScenes, and ResNet50 [10] pretrained on ImageNet [9] for KITTI-360. The numbers of Gaussians are set to 12800 and 38400 in our main results for nuScenes and KITTI-360, respectively. We train our model using AdamW [29] with weight decay of 0.01, and maximum learning rate of 2×10^{-4} , which decays with a cosine annealing schedule. We train our model for 20 epochs on nuScenes with a batch of 8 and 30 epochs on KITTI-360 with a batch size of 4, respectively.

4.3. Main Results

Surround-view 3D semantic occupancy prediction. We report the performance of our GaussianFormer-2 in Table 1. Our approach achieves state-of-the-art performance compared with other methods. Specifically, GaussianFormer-2 surpasses methods based on dense grid representation in classes such as bicycle and motorcycle, proving the flexibility of the proposed probabilistic Gaussian superposition in modeling small objects. Furthermore, our method outperforms GaussianFormer [15] with a clear margin and significantly fewer Gaussians (12800 v.s. 144000), which validates the efficiency and effectiveness of our method.

Table 3. **Ablation on the number of Gaussians.** The latency and memory are tested on an NVIDIA 4090 GPU with batch size one during inference, in accordance with GaussianFormer [15]. We report the latency of the initialization module in parentheses. Our method achieves better performance-efficiency trade-off.

Method	Number of Gaussians	Latency (ms)	Memory (MB)	mIoU	IoU
GaussianFormer	25600	227	4850	16.00	28.72
	144000	372	6229	19.10	29.83
Ours	6400	313 (142)	3026	19.87	30.37
	12800	323 (143)	3041	19.94	30.37
	25600	357 (147)	3063	20.33	31.04

Table 4. **Ablation on the components of GaussianFormer-2.** We set the number of Gaussians to 25600 for these experiments. Depth means using depth as supervision in the initialization module instead of occupancy distribution. Pointcloud represents using ground truth LiDAR scan for initialization.

Probabilistic Modeling	Gaussian Initialization	mIoU	IoU
		16.00	28.72
✓		19.61	30.61
✓	Depth	19.97	30.87
✓	Pointcloud	21.17	34.91
✓	Distribution	<u>20.32</u>	<u>31.04</u>

Monocular 3D semantic occupancy prediction. We report the results for monocular 3D semantic occupancy prediction on SSCBench-KITTI-360 [21] in Table 2. Our method achieves state-of-the-art performance, surpassing the original GaussianFormer in mIoU by 7.6%. To elaborate, we observe significant improvement in mIoU of classes such as road, sidewalk and building compared with GaussianFormer, showing the superiority of probabilistic Gaussian superposition in modeling background stuff.

4.4. Ablation Study

Number of Gaussians. We report the influence of the number of Gaussians on the efficiency and performance of our

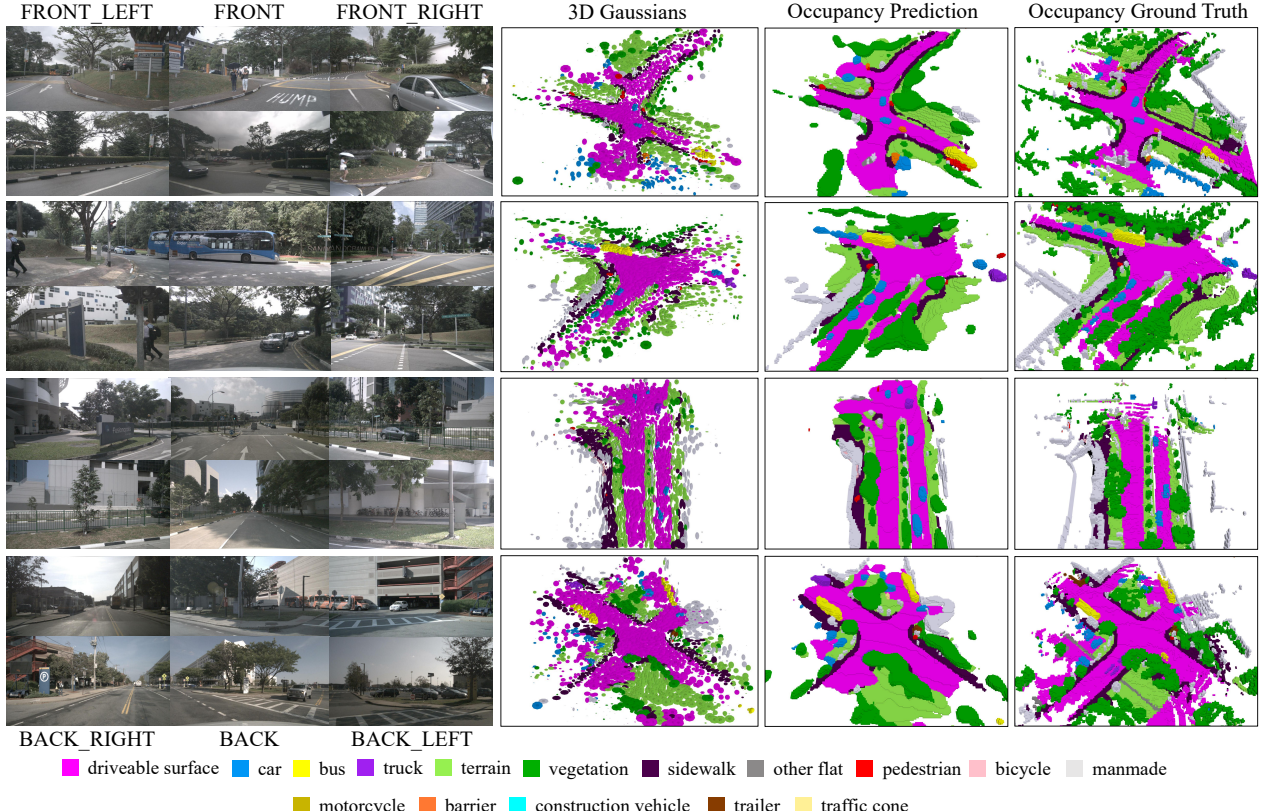


Figure 5. Gaussian and occupancy visualizations on nuScenes. Our model is able to predict both comprehensive and realistic 3D Gaussians and occupancy.

model in Table 3. Our model achieves better performance-efficiency trade-off compared with GaussianFormer, outperforming it with less than 5% number of Gaussians. The latency of our method is higher than GaussianFormer, which we attribute to the time-consuming farthest point sampling (FPS) operation in our initialization module. We adopt the divide-and-conquer strategy to conduct the FPS operation in a batched manner for acceleration, and report the latency of the initialization module in parentheses.

Design Choices. We conduct ablation study on the design choices of GaussianFormer-2 in Table 4. We observe consistent improvement for both probabilistic modeling and distribution-based initialization module which surpasses the depth-based counterpart with a clear margin.

Utilization of Gaussians. We provide comparisons on the utilization of Gaussians between GaussianFormer [15] and our method in Table 5 using two important factors that reflect the utilization of Gaussians, which are position and overlap. Percentage of Gaussians in correct positions (Perc.) is percentage of Gaussians with their mean positions in the occupied space. Overall overlap is calculated as summation of volumes of all Gaussians at 90% over the coverage volume of all Gaussians, while individual overlap is computed by the average of the summation of the Bhattacharyya coefficient of each Gaussian with any other Gaus-

Table 5. Ablation on the efficiency of GaussianFormer-2. We set the number of Gaussians to 25600. Perc. and Dist. denote the percentage of Gaussians in correct positions, and the average distance of each Gaussian to its nearest occupied voxel, respectively. Overall and Indiv. represent the overall and individual overlapping ratios of Gaussians, respectively.

Method	Position		Overlap		mIoU	IoU
	Perc. (%) ↑	Dist. (m) ↓	Overall ↓	Indiv. ↓		
GaussianFormer [15]	16.41	3.07	10.99	68.43	16.00	28.72
Ours	28.85	1.24	3.91	12.48	20.32	31.04

sians. We provide detailed information about these factors in the appendix. Our method outperforms GaussianFormer on all these metrics, demonstrating better utilization.

4.5. Visualizations

We provide Gaussian and occupancy visualizations in Figure 5. Our model is able to predict reasonable Gaussian distributions and comprehensive occupancy results. Further, we compare our method against GaussianFormer in Figure 6. Our Gaussians are more adaptive in shape compared with isotropic spherical Gaussians in GaussianFormer. We also visualize the xy coordinates of Gaussians in the initialization and subsequent blocks of GaussianFormer-2 in Figure 7. We find that the Gaussians successfully learn to move towards occupied area thanks to the object-centric probabilistic design and effective initialization module.

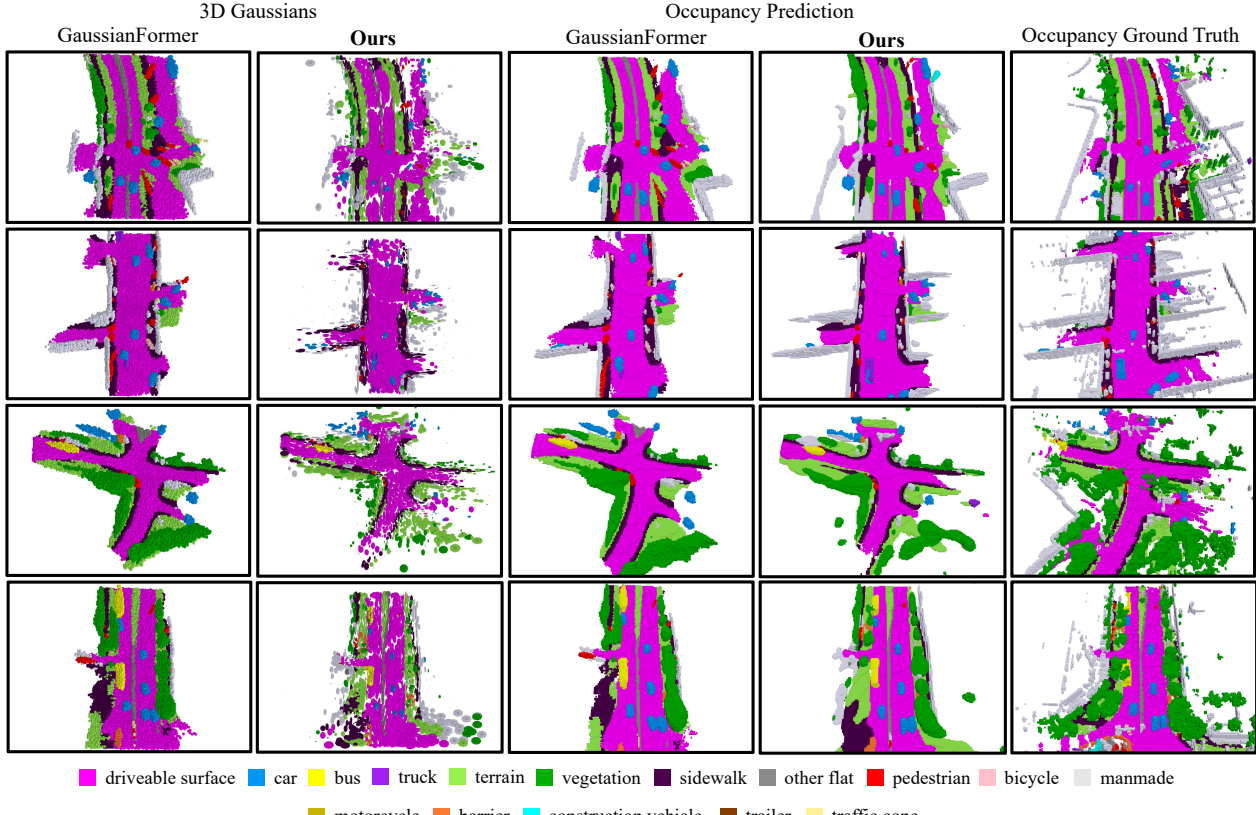


Figure 6. **Comparison with GaussianFormer [15].** Our method predicts 3D Gaussians with more adaptive shapes compared with GaussianFormer. Although our method uses only 8.8% Gaussians, it still generates comprehensive occupancy predictions and alleviates the elongated effect in GaussianFormer.

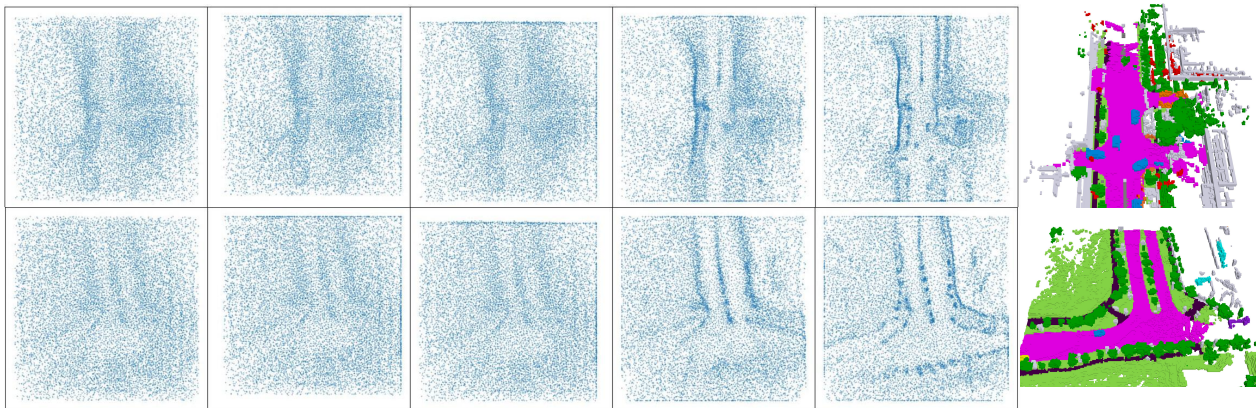


Figure 7. **Visualizations of Gaussian positions in the refinement process.** We observe that our probabilistic Gaussians equipped with distribution-based initialization successfully learn to move towards occupied regions.

5. Conclusion

In this paper, we have proposed a probabilistic Gaussian superposition model as an efficient object-centric representation. Specifically, we interpret each Gaussian as a probability distribution of its neighborhood being occupied and adopt the multiplication theorem of probability to derive the geometry predictions. And we employ the Gaussian mixture model formulation to calculate normalized semantics

predictions. We have also designed a distribution-based initialization strategy to effectively initialize Gaussians around occupied area for object-centric modeling according to pixel-aligned occupancy distribution. Our GaussianFormer-2 has achieved state-of-the-art performance on nuScenes and KITTI-360 datasets for 3D semantic occupancy prediction, which has also demonstrated improved efficiency compared with GaussianFormer on the number of Gaussians, position correctness and overlapping ratio.

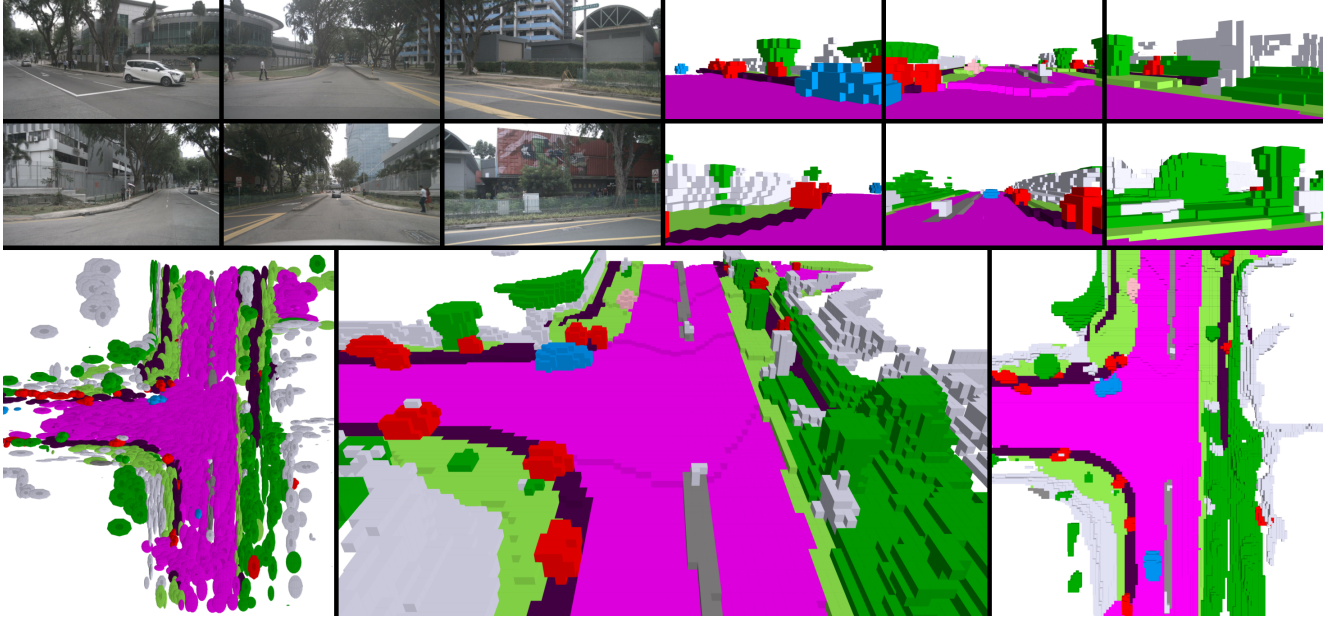


Figure 8. **Visualizations of Gaussians, camera-view and overall occupancy on nuScenes.** We provide the input RGB images and their corresponding camera-view occupancy in the upper part. And we visualize the predicted 3D Gaussians (left), the semantic occupancy in the global view (middle), and in the bird’s eye view (right) in the lower part.

A. Video Demonstration

Figure 8 shows a sampled frame of our video demonstration¹ for 3D semantic occupancy prediction on the nuScenes dataset [2]. We note that the camera-view occupancy visualizations align well with the input RGB images. Moreover, each instance is sparsely described by only a few Gaussians with adaptive shapes, which demonstrates the efficiency and the object-centric nature of our model.

B. Visualizations on KITTI-360

We provide visualization results of Gaussians and occupancy on the KITTI-360 dataset [26] in Figure 9. We observe that our GaussianFormer-2 is able to predict both intricate geometry and semantics of the 3D scene. Furthermore, the 3D Gaussians in our model are adaptive in their scales according to the specific objects they are describing, compared with isotropic spherical Gaussians with maximum scales in GaussianFormer [15].

C. Metric Details

Position. Gaussians, even after full training, can still be found in unoccupied space due to the localized nature of the receptive field. These Gaussians fail to describe meaningful structures, rendering them ineffective and devoid of practical utility. A higher proportion of Gaussians in unoccupied space indicates suboptimal utilization. Hence, we define the

percentage of Gaussians in correct positions (Perc.) as:

$$\text{Perc.} = \frac{N_{\text{correct}}}{N_{\text{total}}} \cdot 100\%, \quad (12)$$

where N_{correct} , and N_{total} denote the number of Gaussians of which means are in occupied space, and the total number of Gaussians, respectively. A higher percentage indicates a better alignment of the Gaussians with occupied or meaningful area in the space, thus reflecting a more efficient use of the model’s capacity.

The above measurement provides a hard evaluation, where Gaussians are either classified as being in correct or incorrect positions without considering their proximity to the nearest occupied area. This binary approach does not capture how close Gaussians in unoccupied regions are to meaningful positions. To address this limitation, we define a complementary soft measurement as the average distance of each Gaussian to its nearest occupied voxel center, denoted as Dist. (in meters), computed as follows:

$$\text{Dist.} = \frac{1}{P} \sum_{i=1}^P \min_{\mathbf{v} \in \mathcal{V}} \|\mathbf{m}_i - \mathbf{v}\|_1, \quad (13)$$

where \mathbf{m}_i , \mathcal{V} , \mathbf{v} , and $\|\mathbf{m}_i - \mathbf{v}\|_1$ denote the mean of the i -th Gaussian, the set of occupied voxel centers, the center of one voxel in this set, and L1 distance between the mean of the Gaussian and the voxel center, respectively. Note that this distance is calculated with respect to the voxel center, and thus Gaussians positioned within the correct occupied area may also have a non-zero distance.

¹<https://github.com/huang-yh/GaussianFormer>

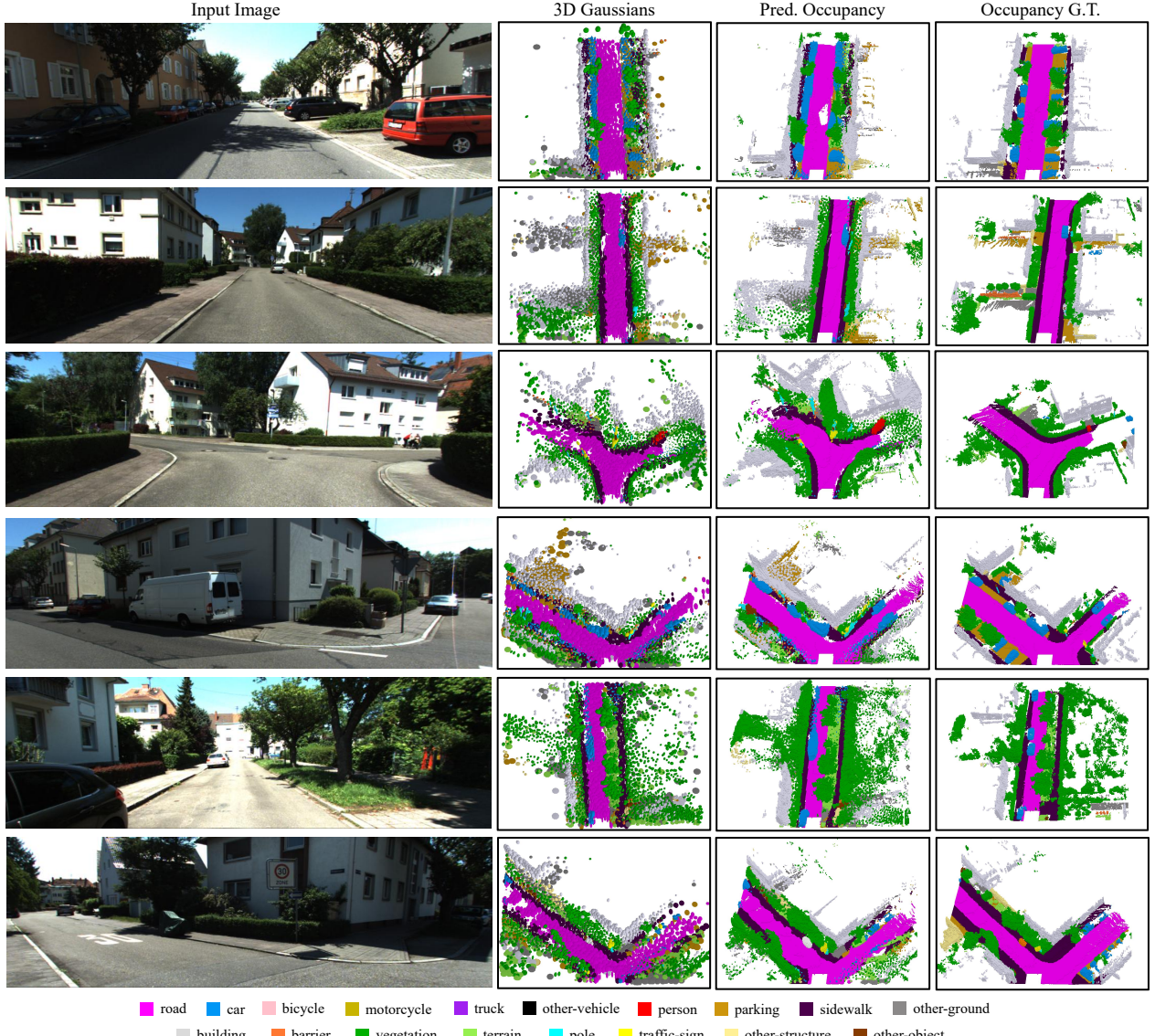


Figure 9. **Visualizations of Gaussians and occupancy on KITTI-360.** Our method captures both the intricate geometry and semantics of the scene with shape-adaptive Gaussians.

Overlap. The *overall overlapping ratio of Gaussians (Overall.)* provides a global perspective on the redundancy in the Gaussian representation. Each Gaussian is modeled as an ellipsoid, where the semi-axis lengths are derived from the Mahalanobis distance at a chi-squared value of 6.251, corresponding to the 90% confidence level of a Gaussian distribution in three degrees of freedom (DoFs). The *Overall.* is then calculated as the ratio of the summed 90% confidence volumes $V_{i,90\%}$ of all Gaussians to the total coverage volume of all Gaussians V_{coverage} in the scene:

$$\text{Overall.} = \frac{\sum_{i=1}^P V_{i,90\%}}{V_{\text{coverage}}}, \quad (14)$$

where V_{coverage} represents the volume of all Gaussians combined as a unified shape. To estimate V_{coverage} , we employ

the *Monte Carlo method* where a large number of points are randomly sampled within the bounding box of the scene. For each sampled point, we check whether it lies within the 90% confidence ellipsoid of any Gaussian. The volume is then approximated as:

$$V_{\text{coverage}} = V_{\text{scene}} \cdot \frac{N_{\text{in}}}{N_{\text{total}}}, \quad (15)$$

where N_{in} , and N_{total} are the number of sampled points that fall within the 90% confidence ellipsoid of at least one Gaussian, and the total number of sampled points, respectively. This approach ensures an accurate estimation of the unified volume, efficiently handling the overlapping regions of the Gaussians by not double-counting them.

We next detail the derivation of the ellipsoid volume cor-

responding to the 90% confidence region of a 3D Gaussian distribution. Considering a multivariate Gaussian distribution in 3D defined as:

$$g(\mathbf{x}) = \frac{1}{(2\pi)^{3/2}|\Sigma|^{1/2}} \exp\left(-\frac{1}{2}(\mathbf{x}-\mathbf{m})^T \Sigma^{-1} (\mathbf{x}-\mathbf{m})\right), \quad (16)$$

where \mathbf{x} , Σ , and $|\Sigma|$ are the mean vector, 3x3 covariance matrix, and the determinant of the covariance matrix, respectively. The *Mahalanobis distance* d of point \mathbf{x} from the mean \mathbf{m} is defined as:

$$d^2(\mathbf{x}, \mathbf{m}) = (\mathbf{x} - \mathbf{m})^T \Sigma^{-1} (\mathbf{x} - \mathbf{m}). \quad (17)$$

The 90% confidence region of the Gaussian distribution corresponds to the set of points for which the Mahalanobis distance satisfies:

$$d^2 \leq \chi_{3,0.9}^2 \approx 6.251, \quad (18)$$

where $\chi_{3,0.9}^2$ is the chi-square critical value for three degrees of freedom at the 90% confidence level. For a Gaussian distribution, the semi-axis lengths are determined by the square root of the eigenvalues of Σ , scaled by $\chi_{3,0.9}^2$. Thus, the volume of the ellipsoid from 90% of the 3D Gaussian distribution is:

$$V_{90\%} = \frac{4}{3}\pi(6.251)^{3/2}|\Sigma|^{1/2}. \quad (19)$$

A higher value of *Overall* indicates greater overlapping volumes among the Gaussians, signifying redundancy in Gaussian representation. This metric provides insights into the utilization of Gaussians to represent the scene.

The *individual overlapping ratio of Gaussians (Indiv.)* offers a fine-grained analysis of the overlap between Gaussians in a scene. This measurement quantifies the degree to which each Gaussian overlaps with all other Gaussians, averaged across all Gaussians in the scene. The value of this metric indicates approximately how many times the volume of a single Gaussian is fully overlapped with other Gaussians on average. To compute this, we use the Bhattacharyya coefficient [1], which measures the similarity between two Gaussian distributions. The *individual overlapping ratio* is defined as:

$$\text{Indiv.} = \frac{1}{P} \sum_{i=1}^P \left(\sum_{j \neq i} \text{BC}_{i,j} \right), \quad (20)$$

where $\text{BC}_{i,j}$ is the Bhattacharyya coefficient between the i -th and j -th Gaussians, given by:

$$\text{BC}_{i,j} = \frac{\sqrt[4]{\Sigma_i || \Sigma_j |}}{\sqrt{|\Sigma_{ij}|}} e^{-\frac{1}{8}(\mathbf{m}_i - \mathbf{m}_j)^T \Sigma_{ij}^{-1} (\mathbf{m}_i - \mathbf{m}_j)}, \quad (21)$$

where $\Sigma_{ij} = \frac{1}{2}(\Sigma_i + \Sigma_j)$ is the average covariance matrix. A higher value of *Indiv.* indicates more redundancy, as Gaussians are heavily overlapping with each other.

References

- [1] Anil Bhattacharyya. On a measure of divergence between two statistical populations defined by their probability distribution. *Bulletin of the Calcutta Mathematical Society*, 35:99–110, 1943. 11
- [2] Holger Caesar, Varun Bankiti, Alex H Lang, Sourabh Vora, Venice Erin Liang, Qiang Xu, Anush Krishnan, Yu Pan, Giancarlo Baldan, and Oscar Beijbom. nuscenes: A multimodal dataset for autonomous driving. In *CVPR*, 2020. 2, 5, 6, 9
- [3] Anh-Quan Cao and Raoul de Charette. Monoscene: Monocular 3d semantic scene completion. In *CVPR*, pages 3991–4001, 2022. 1, 2, 3, 5, 6
- [4] Anh-Quan Cao and Raoul de Charette. Scenerf: Self-supervised monocular 3d scene reconstruction with radiance fields. In *ICCV*, pages 9387–9398, 2023. 1
- [5] Xiaozhi Chen, Huimin Ma, Ji Wan, Bo Li, and Tian Xia. Multi-view 3d object detection network for autonomous driving. In *CVPR*, pages 1907–1915, 2017. 2
- [6] Xiaokang Chen, Kwan-Yee Lin, Chen Qian, Gang Zeng, and Hongsheng Li. 3d sketch-aware semantic scene completion via semi-supervised structure prior. In *CVPR*, 2020. 2
- [7] Yueh-Tung Chen, Martin Garbade, and Juergen Gall. 3d semantic scene completion from a single depth image using adversarial training. In *ICIP*, pages 1835–1839. IEEE, 2019. 2
- [8] Ran Cheng, Ryan Razani, Ehsan Taghavi, Enxu Li, and Bingbing Liu. 2-s3net: Attentive feature fusion with adaptive feature selection for sparse semantic segmentation network. In *CVPR*, pages 12547–12556, 2021. 2
- [9] Jia Deng, Wei Dong, Richard Socher, Li-Jia Li, Kai Li, and Li Fei-Fei. Imagenet: A large-scale hierarchical image database. In *CVPR*, pages 248–255. Ieee, 2009. 6
- [10] Kaiming He, Xiangyu Zhang, Shaoqing Ren, and Jian Sun. Deep residual learning for image recognition. In *CVPR*, 2016. 6
- [11] Yihan Hu, Jiazhi Yang, Li Chen, Keyu Li, Chonghao Sima, Xizhou Zhu, Siqi Chai, Senyao Du, Tianwei Lin, Wenhui Wang, et al. Goal-oriented autonomous driving. *arXiv preprint arXiv:2212.10156*, 2022. 1
- [12] Junjie Huang, Guan Huang, Zheng Zhu, and Da-long Du. Bevdet: High-performance multi-camera 3d object detection in bird-eye-view. *arXiv preprint arXiv:2112.11790*, 2021. 2, 5
- [13] Yuanhui Huang, Wenzhao Zheng, Yunpeng Zhang, Jie Zhou, and Jiwen Lu. Tri-perspective view for vision-based 3d semantic occupancy prediction. In *CVPR*, pages 9223–9232, 2023. 1, 2, 3, 5, 6

- [14] Yuanhui Huang, Wenzhao Zheng, Borui Zhang, Jie Zhou, and Jiwen Lu. Selfocc: Self-supervised vision-based 3d occupancy prediction. In *CVPR*, 2024. 1
- [15] Yuanhui Huang, Wenzhao Zheng, Yunpeng Zhang, Jie Zhou, and Jiwen Lu. Gaussianformer: Scene as gaussians for vision-based 3d semantic occupancy prediction. *arXiv preprint arXiv:2405.17429*, 2024. 1, 2, 3, 5, 6, 7, 8, 9
- [16] Bo Jiang, Shaoyu Chen, Qing Xu, Bencheng Liao, Jiajie Chen, Helong Zhou, Qian Zhang, Wenyu Liu, Chang Huang, and Xinggang Wang. Vad: Vectorized scene representation for efficient autonomous driving. *arXiv preprint arXiv:2303.12077*, 2023. 1
- [17] Haoyi Jiang, Tianheng Cheng, Naiyu Gao, Haoyang Zhang, Wenyu Liu, and Xinggang Wang. Symphonize 3d semantic scene completion with contextual instance queries. *arXiv preprint arXiv:2306.15670*, 2023. 1
- [18] Alex H Lang, Sourabh Vora, Holger Caesar, Lubing Zhou, Jiong Yang, and Oscar Beijbom. Pointpillars: Fast encoders for object detection from point clouds. In *CVPR*, pages 12697–12705, 2019. 2
- [19] Jie Li, Kai Han, Peng Wang, Yu Liu, and Xia Yuan. Anisotropic convolutional networks for 3d semantic scene completion. In *CVPR*, 2020. 2
- [20] Yinhao Li, Zheng Ge, Guanyi Yu, Jinrong Yang, Zengran Wang, Yukang Shi, Jianjian Sun, and Zeming Li. Bevdepth: Acquisition of reliable depth for multi-view 3d object detection. *arXiv preprint arXiv:2206.10092*, 2022. 1, 2, 5
- [21] Yiming Li, Sihang Li, Xinhao Liu, Moonjun Gong, Kenan Li, Nuo Chen, Zijun Wang, Zhiheng Li, Tao Jiang, Fisher Yu, et al. Sscbench: A large-scale 3d semantic scene completion benchmark for autonomous driving. *arXiv preprint arXiv:2306.09001*, 2023. 5, 6
- [22] Yiming Li, Zhiding Yu, Christopher Choy, Chaowei Xiao, Jose M Alvarez, Sanja Fidler, Chen Feng, and Anima Anandkumar. Voxformer: Sparse voxel transformer for camera-based 3d semantic scene completion. In *CVPR*, pages 9087–9098, 2023. 1, 2, 5, 6
- [23] Zhiqi Li, Wenhui Wang, Hongyang Li, Enze Xie, Chonghao Sima, Tong Lu, Qiao Yu, and Jifeng Dai. Bevformer: Learning bird’s-eye-view representation from multi-camera images via spatiotemporal transformers. *arXiv preprint arXiv:2203.17270*, 2022. 1, 2, 5
- [24] Zhiqi Li, Zhiding Yu, David Austin, Mingsheng Fang, Shiyi Lan, Jan Kautz, and Jose M Alvarez. Fb-occ: 3d occupancy prediction based on forward-backward view transformation. *arXiv preprint arXiv:2307.01492*, 2023. 1, 2
- [25] Tingting Liang, Hongwei Xie, Kaicheng Yu, Zhongyu Xia, Zhiwei Lin, Yongtao Wang, Tao Tang, Bing Wang, and Zhi Tang. Bevfusion: A simple and robust lidar-camera fusion framework. *NIPS*, 35:10421–10434, 2022. 2
- [26] Yiyi Liao, Jun Xie, and Andreas Geiger. KITTI-360: A novel dataset and benchmarks for urban scene understanding in 2d and 3d. *PAMI*, 2022. 2, 5, 6, 9
- [27] Venice Erin Liong, Thi Ngoc Tho Nguyen, Sergi Widjaja, Dhananjai Sharma, and Zhuang Jie Chong. Amvnet: Assertion-based multi-view fusion network for lidar semantic segmentation. *arXiv preprint arXiv:2012.04934*, 2020. 2
- [28] Zhijian Liu, Haotian Tang, Alexander Amini, Xinyu Yang, Huizi Mao, Daniela L Rus, and Song Han. Bevfusion: Multi-task multi-sensor fusion with unified bird’s-eye view representation. In *ICRA*, pages 2774–2781. IEEE, 2023. 2
- [29] Ilya Loshchilov and Frank Hutter. Decoupled weight decay regularization. *arXiv preprint arXiv:1711.05101*, 2017. 6
- [30] Yuhang Lu, Xinge Zhu, Tai Wang, and Yuexin Ma. Octreeocc: Efficient and multi-granularity occupancy prediction using octree queries. *arXiv preprint arXiv:2312.03774*, 2023. 2
- [31] Ruihang Miao, Weizhou Liu, Mingrui Chen, Zheng Gong, Weixin Xu, Chen Hu, and Shuchang Zhou. Ocdepth: A depth-aware method for 3d semantic scene completion. *arXiv preprint arXiv:2302.13540*, 2023. 1
- [32] Zak Murez, Tarrence Van As, James Bartolozzi, Ayan Sinha, Vijay Badrinarayanan, and Andrew Rabinovich. Atlas: End-to-end 3d scene reconstruction from posed images. In *ECCV*, pages 414–431. Springer, 2020. 5
- [33] Jonah Philion and Sanja Fidler. Lift, splat, shoot: Encoding images from arbitrary camera rigs by implicitly unprojecting to 3d. In *ECCV*, 2020. 2
- [34] Luis Roldão, Raoul de Charette, and Anne Verroust-Blondet. Lmscnet: Lightweight multiscale 3d semantic completion. In *ThreeDV*, 2020. 2, 6
- [35] Yang Shi, Tianheng Cheng, Qian Zhang, Wenyu Liu, and Xinggang Wang. Occupancy as set of points. In *ECCV*, 2024. 3
- [36] Shuran Song, Fisher Yu, Andy Zeng, Angel X Chang, Manolis Savva, and Thomas Funkhouser. Semantic scene completion from a single depth image. In *CVPR*, pages 1746–1754, 2017. 6
- [37] Haotian Tang, Zhijian Liu, Shengyu Zhao, Yujun Lin, Ji Lin, Hanrui Wang, and Song Han. Searching efficient 3d architectures with sparse point-voxel convolution. In *ECCV*, pages 685–702. Springer, 2020. 2
- [38] Pin Tang, Zhongdao Wang, Guoqing Wang, Jilai Zheng, Xiangxuan Ren, Bailan Feng, and Chao Ma. Sparseocc: Rethinking sparse latent representation

- for vision-based semantic occupancy prediction. In *CVPR*, pages 15035–15044, 2024. 2
- [39] Xiaoyu Tian, Tao Jiang, Longfei Yun, Yue Wang, Yilun Wang, and Hang Zhao. Occ3d: A large-scale 3d occupancy prediction benchmark for autonomous driving. *arXiv preprint arXiv:2304.14365*, 2023. 1, 2
- [40] Wenwen Tong, Chonghao Sima, Tai Wang, Li Chen, Silei Wu, Hanming Deng, Yi Gu, Lewei Lu, Ping Luo, Dahua Lin, et al. Scene as occupancy. In *ICCV*, pages 8406–8415, 2023. 1
- [41] Jiabao Wang, Zhaojiang Liu, Qiang Meng, Liujiang Yan, Ke Wang, Jie Yang, Wei Liu, Qibin Hou, and Mingming Cheng. Opus: occupancy prediction using a sparse set. In *NIPS*, 2024. 3
- [42] Lening Wang, Wenzhao Zheng, Yilong Ren, Han Jiang, Zhiyong Cui, Haiyang Yu, and Jiwen Lu. Occsora: 4d occupancy generation models as world simulators for autonomous driving. *arXiv preprint arXiv:2405.20337*, 2024. 1
- [43] Tai Wang, Xinge Zhu, Jiangmiao Pang, and Dahua Lin. Fcos3d: Fully convolutional one-stage monocular 3d object detection. In *ICCV*, pages 913–922, 2021. 6
- [44] Yi Wei, Linqing Zhao, Wenzhao Zheng, Zheng Zhu, Jie Zhou, and Jiwen Lu. Surroundocc: Multi-camera 3d occupancy prediction for autonomous driving. In *ICCV*, pages 21729–21740, 2023. 1, 2, 5
- [45] Felix Wimbauer, Nan Yang, Christian Rupprecht, and Daniel Cremers. Behind the scenes: Density fields for single view reconstruction. In *CVPR*, pages 9076–9086, 2023. 1
- [46] Xu Yan, Jiantao Gao, Jie Li, Ruimao Zhang, Zhen Li, Rui Huang, and Shuguang Cui. Sparse single sweep lidar point cloud segmentation via learning contextual shape priors from scene completion. In *AAAI*, pages 3101–3109, 2021. 2
- [47] Ziyang Yan, Wenzhen Dong, Yihua Shao, Yuhang Lu, Liu Haiyang, Jingwen Liu, Haozhe Wang, Zhe Wang, Yan Wang, Fabio Remondino, et al. Renderworld: World model with self-supervised 3d label. *arXiv preprint arXiv:2409.11356*, 2024. 1
- [48] Dongqiangzi Ye, Zixiang Zhou, Weijia Chen, Yufei Xie, Yu Wang, Panqu Wang, and Hassan Foroosh. Lidarmultinet: Towards a unified multi-task network for lidar perception. In *AAAI*, pages 3231–3240, 2023. 2
- [49] Maosheng Ye, Rui Wan, Shuangjie Xu, Tongyi Cao, and Qifeng Chen. Drinet++: Efficient voxel-as-point point cloud segmentation. *arXiv preprint arXiv:2111.08318*, 2021. 2
- [50] Zichen Yu, Changyong Shu, Jiajun Deng, Kangjie Lu, Zongdai Liu, Jiangyong Yu, Dawei Yang, Hui Li, and Yan Chen. Flashocc: Fast and memory-efficient occupancy prediction via channel-to-height plugin. *arXiv preprint arXiv:2311.12058*, 2023. 1, 2
- [51] Yunpeng Zhang, Zheng Zhu, and Dalong Du. Ocformer: Dual-path transformer for vision-based 3d semantic occupancy prediction. *arXiv preprint arXiv:2304.05316*, 2023. 1, 5, 6
- [52] Wenzhao Zheng, Weiliang Chen, Yuanhui Huang, Borui Zhang, Yueqi Duan, and Jiwen Lu. Occworld: Learning a 3d occupancy world model for autonomous driving. *arXiv preprint arXiv:2311.16038*, 2023. 1
- [53] Yin Zhou and Oncel Tuzel. Voxelnet: End-to-end learning for point cloud based 3d object detection. In *CVPR*, pages 4490–4499, 2018. 2